01 May 2015

Determining Crustal Structure beneath Seismic Stations Overlying a Low-Velocity Sedimentary Layer using Receiver Functions

Youqiang Yu

Jianguo Song

Kelly H. Liu
Missouri University of Science and Technology, liukh@mst.edu

Stephen S. Gao
Missouri University of Science and Technology, sgao@mst.edu

Recommended Citation

Key Points:
- We proposed a technique to remove sedimentary effects
- We extended the conventional *H-k* stacking method
- Our technique can determine both sedimentary and crustal structures

Correspondence to:
Y. Yu,
yyqkc@mst.edu

Determining crustal structure beneath seismic stations overlying a low-velocity sedimentary layer using receiver functions

**Youqiang Yu[1], Jianguo Song[1,2], Kelly H. Liu[1], and Stephen S. Gao[1]**

[1]Geology and Geophysics Program, Missouri University of Science and Technology, Rolla, Missouri, USA, [2]School of Geosciences, China University of Petroleum, Qingdao, China

Abstract The receiver function (RF) technique has been widely applied to investigate crustal and mantle layered structures using *P*-to-*S* converted (*Ps*) phases from velocity discontinuities. However, the presence of low-velocity (relative to that of the bedrock) sediments can give rise to strong reverberations in the resulting RFs, frequently masking the *Ps* phases from crustal and mantle boundaries. Such reverberations are caused by *P*-to-*S* conversions and their multiples associated with the strong impedance contrast across the bottom of the low-velocity sedimentary layer. Here we propose and test an approach to effectively remove the near-surface reverberations and decipher the *Ps* phases associated with the Moho discontinuity. Autocorrelation is first applied on the observed RFs to determine the strength and two-way traveltime of the reverberations, which are then used to construct a resonance removal filter in the frequency domain to remove or significantly reduce the reverberations. The filtered RFs are time corrected to eliminate the delay effects of the sedimentary layer and applied to estimate the subsediment crustal thickness and V_P/V_S using a *H-k* stacking procedure. The resulting subsediment crustal parameters (thickness and V_P/V_S) are subsequently used to determine the thickness and V_P/V_S of the sedimentary layer, using a revised version of the *H-k* stacking procedure. Testing using both synthetic and real data suggests that this computationally inexpensive technique is efficient in resolving subsediment crustal properties beneath stations sitting on a low-velocity sedimentary layer and can also satisfactorily determine the thickness and V_P/V_S of the sedimentary layer.

1. Introduction

P-to-*S* converted phases and their multiples (hereafter collectively called the *Ps* phases) related to the Moho including *PmS*, *PPmS*, and *PSmS* (Figure 1) have been widely employed to image crustal thickness and V_P/V_S beneath a recording site using the receiver function (RF) technique [*Langston*, 1979; *Owens et al.*, 1984; *Ammon*, 1991; *Zandt and Ammon*, 1995; *Zhu and Kanamori*, 2000]. However, the existence of a low-velocity sedimentary layer poses significant problems to successfully apply the RF technique [*Zelt and Ellis*, 1999]. The large acoustic impedance (product of velocity and density) contrast between the low-velocity sedimentary layer and the crystalline crust can give rise to strong *P*-to-*S* wave conversions and near-surface reverberations, significantly masking the *Ps* phases associated with the Moho [*Langston*, 2011]. Consequently, the conventional *H-k* (crustal thickness-V_P/V_S) stacking technique [*Zhu and Kanamori*, 2000] usually leads to erroneous results. *Yeck et al.* [2013] estimated that a deep basin could contribute to an error of more than 10 km in the resulting crustal thickness if the sedimentary effects are not correctly accounted for.

A variety of teleseismic techniques have been proposed and developed for the purpose of determining both the sedimentary and crustal structures. Forward modeling was conducted to obtain sedimentary and crustal *S* wave velocity models by iteratively fitting the synthetics to the observed RFs [*Sheehan et al.*, 1995; *Zelt and Ellis*, 1999; *Clitheroe et al.*, 2000; *Anandakrishnan and Winberry*, 2004; *Mandal*, 2006; *He et al.*, 2012], but the strong near-surface reverberations on the resulting radial RFs make it difficult to reliably determine the best fitting synthetics [*Clitheroe et al.*, 2000]. *Langston* [2011] used the bedrock structure of stations close to the sedimentary area as a priori crustal parameters to isolate the upgoing *S* wavefield from the total teleseismic response of the *P* wave for stations within the sedimentary basin, using the theory of wavefield continuation and decomposition [*Thorwart and Dahm*, 2005; *Bostock and Trehu*, 2012]. Recently, *Tao et al.* [2014] improved the technique of *Langston* [2011] by minimizing the upgoing *S* wave energy without the need for the
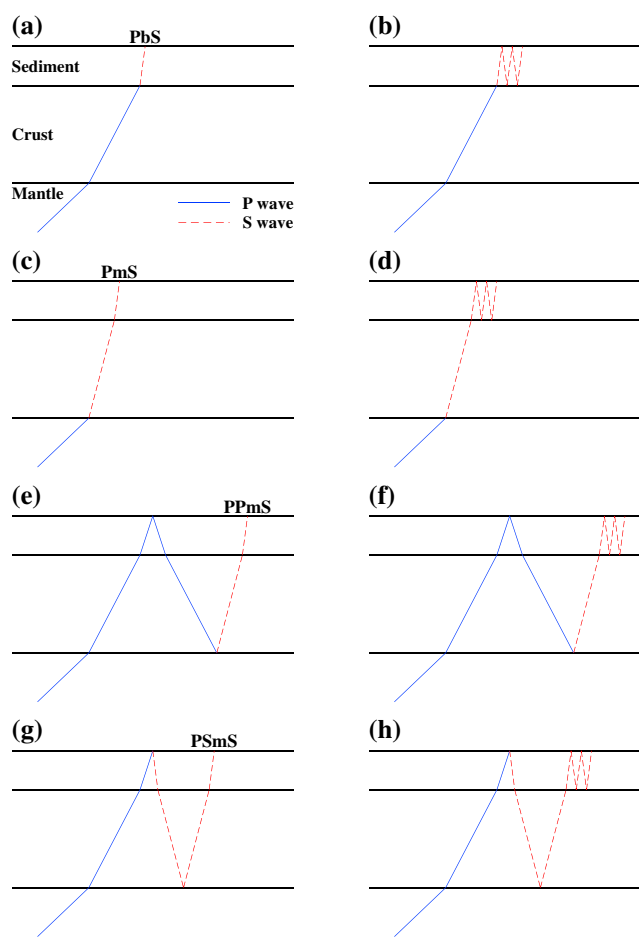
Figure 1. Schematic diagrams showing (a, c, e, and g) the main *Ps* phases and (b, d, f, and h) their reverberations in the sedimentary layer.

reference stations. The computationally intensive approach of wavefield continuation and decomposition is effective in obtaining reliable crustal parameters beneath sedimentary basins, under the condition when the densities and *P* wave velocities of the involved layers (sediment, crust, and mantle) are known. *Yeck et al.* [2013] proposed a sequential two-layer *H-k* stacking method to determine the sedimentary and crustal struc-tures. This technique works the best when the Moho *Ps* phases are not entirely masked by the sedimentary reverberations [*Yeck et al.*, 2013]. In addition, some recent studies attempted to reduce the influence of the sedimentary layer by applying band-pass or band-rejection filters [*Leahy et al.*, 2012; *Reed et al.*, 2014], but it is sometimes subjective to decide the optimal frequency bands, and the removal of the sedimentary effects is frequently incomplete.

Although reverberations associated with a low-velocity sedimentary layer can partially or totally mask the Moho *Ps* phases, as described below, we find that they can be effectively removed or significantly reduced by applying a resonance removal filter. The parameters needed to construct the filter are taken directly from the observed RFs. The filtered RFs are then utilized to obtain subsediment crustal thickness and V_P/V_S and are subsequently used to obtain the thickness and V_P/V_S of the sedimentary layer. Similar to the standard *H-k* stacking technique [*Zhu and Kanamori*, 2000], the approach requires *P* wave velocities but not the densities of the involved layers.

2. Methods

2.1. Receiver Function
Teleseismic waves travel through the interior of the Earth and are recorded by seismic stations at the surface. The conversion from compressional to shear waves occurs when *P* waves encounter an acoustic impedance

interface within the Earth. The recorded seismic waveforms are the combined results of the source time function, travel path, and local structure [*Burdick and Langston*, 1977; *Langston*, 1979]. Due to the steep angle of incidence of teleseismic waves near the surface, most of the shear wave energy is recorded in the radial component while the vertical component is predominantly occupied by the compressional wave. The *Ps* phases can be source normalized by deconvolving the vertical component from the corresponding section of the radial component [*Ammon*, 1991]. The resulting time series reflect the relative responses of the Earth's structure near the receiver and are named as receiver functions [*Langston*, 1979]. The receiver functions used in the study were generated by employing the water level deconvolution technique [*Ammon*, 1991], which is a division in the frequency domain, with a water level of 0.05 and a Gaussian width factor of 5.0.

The *Ps* phases in the resulting RFs can be expressed as [*Ammon*, 1991]

$$F(t) = A_s \delta(t - t_s), \tag{1}$$

where $\delta(t - t_s)$ is a Dirac delta function and A_s and t_s represent the corresponding amplitudes and time delays, respectively, of the *Ps* phases (including direct conversions such as *PmS* and multiples such as *PPmS* and *PSmS*; see Figure 1). The reference time ($t = 0$) corresponds to the arrival time of the direct *P* wave. A popularly used procedure for crustal studies using RFs is *H-k* stacking, in which the radial RFs are moveout corrected and stacked along the traveltime curves of the Moho *Ps* phases at each candidate pair of *H* (thickness) and *k* (V_P/V_S) in a grid search procedure [*Chevrot and Van der Hilst*, 2000; *Zhu and Kanamori*, 2000; *Nair et al.*, 2006; *Bashir et al.*, 2011]. The maximum stacking amplitude corresponds to the optimal crustal thickness and V_P/V_S.

2.2. Effects of a Low-Velocity Sedimentary Layer

It has long been recognized that a low-velocity sedimentary layer of a few kilometers or thinner (Figure 1) can result in prominent high-amplitude, low-frequency reverberations. Relative to RFs recorded by stations on bedrock, the width of the first *P* arrival is broadened and its amplitude is decreased [*Zelt and Ellis*, 1999]. On the RFs, the amplitude of the first *Ps* phase from the bottom of the sedimentary layer (hereafter named *PbS* phase, with one *S* wave leg in the sedimentary layer; see Figure 1a) can become so high that the direct *P* wave is usually completely masked. Such RFs are characterized by a delayed first peak corresponding to the arrival of the *PbS* [*Yeck et al.*, 2013] (Figure 2a).

The large impedance contrasts across the bottom of the sedimentary layer and that from the free surface create strong reverberations in the form of multiples. Similar to multiples created in a water layer [e.g., *Stoffa et al.*, 1974, equation (18)], for a model with a low-velocity sedimentary layer (Figure 1), the primary and multiples of the converted shear waves can be expressed as

$$H(t) = \sum_{n=0}^{\infty} (-r_0)^n \times F(t - n \times \Delta t), \tag{2}$$

where n is the index of the nth reverberation of the converted shear phases, r_0 is the strength (proportional to the reflection coefficient at the bottom of the sedimentary layer) of the near-surface reverberations, Δt is the two-way traveltime for the reverberations of the converted waves in the sedimentary layer, and $F(t)$ is the RF without the influence of the sedimentary layer (equation (1)). Note that for $n = 0$, $H(t)$ equals $F(t)$ and represents the primary arrivals, and for $n = 1$ (the first reverberation), the arrivals have a negative polarity (due to the reflection from the free surface) and a delay time of Δt relative to the direct phase. Due to the steep incident angle of *PbS* and the large acoustic impedance contrast across the bottom of the sedimentary layer, the dominant energy in the RFs is the reverberations of *PbS*, followed by those of *PmS*, *PPmS*, and *PSmS* in the sedimentary layer (Figure 1). Synthetic tests show that *PPbS* and *PSbS* and their reverberations are much weaker than the corresponding *PbS* phases, mostly because of the near-vertical raypaths associated with the small sedimentary velocities and the consequent inefficiency in producing converted *S* waves.

In the frequency domain, equation (2) can be expressed as

$$H(i\omega) = F(i\omega) \sum_{n=0}^{\infty} (-r_0)^n e^{-i\omega n \Delta t}, \tag{3}$$

where i is the complex symbol and $\sum_{n=0}^{\infty} (-r_0)^n e^{-i\omega n \Delta t}$ is a geometric series that can be simplified as $(1 + r_0 e^{-i\omega \Delta t})^{-1}$. Thus, $F(t)$ can be obtained in the frequency domain using

$$F(i\omega) = H(i\omega)(1 + r_0 e^{-i\omega \Delta t}). \tag{4}$$
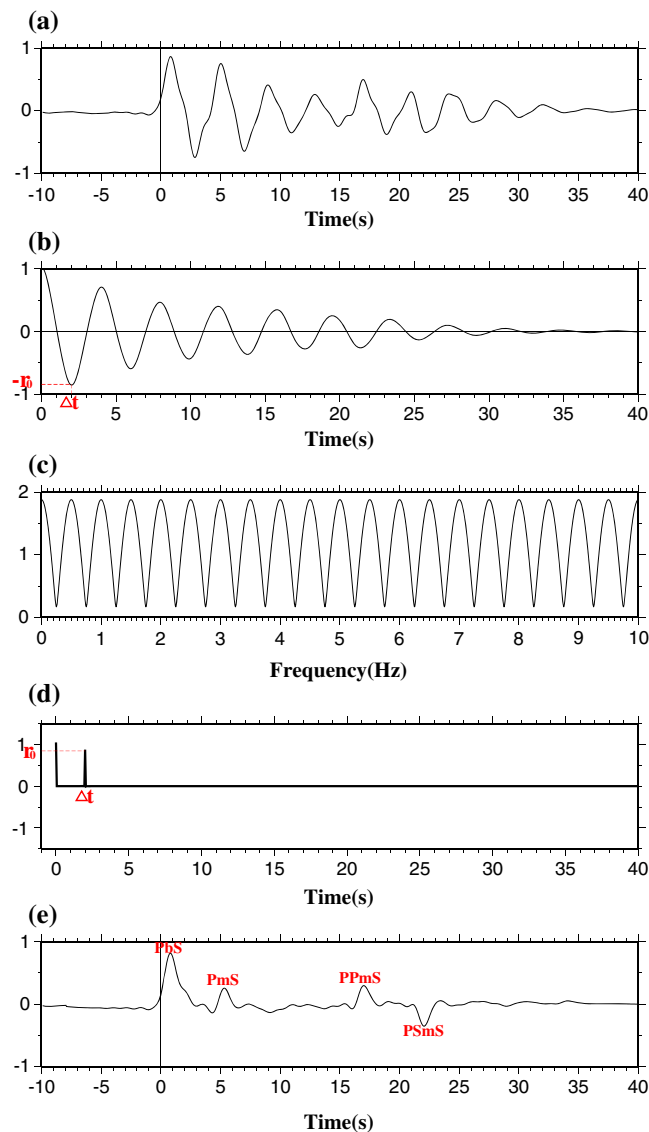
Figure 2. (a) Synthetic RF. Note that the first peak is delayed by about 1 s and represents the *P*-to-*S* converted phase from the bottom of the sedimentary layer. (b) Autocorrelation of the RF shown in Figure 2a. Δt and r_0 are the two-way traveltime and strength of the sedimentary reverberations, respectively. (c) Frequency domain plot of a resonance removal filter with $r_0 = 0.8$ and $\Delta t = 2.0$ s. (d) Same as Figure 2c but in the time domain. (e) Resulting RF after applying the resonance removal filter.

$F(i\omega)$ is the RF in the frequency domain after the removal of the sedimentary reverberations. Using the above equation, near-surface reverberations can be eliminated from the observed RF spectrum ($H(i\omega)$) by designing a resonance removal filter of the form ($1 + r_0 e^{-i\omega\Delta t}$). An example of such a filter in both the frequency and time domains is shown in Figure 2. Such a filter has been widely applied in petroleum exploration to quantify and remove multiples especially those associated with a surface water layer [*Stoffa et al.*, 1974; *Yilmaz*, 2001].

The strength of the reverberations (r_0) required by the filter can be directly measured from the original RFs (Figure 2a) as the ratio between the amplitude of the first trough and that of the first peak, and the two-way traveltime (Δt) can be measured using the time separation between the first peak and first trough. However, as routinely used in exploration seismology [e.g., *Yilmaz*, 2001], they can be more reliably determined from the normalized autocorrelation function (Figure 2b), which has a unity amplitude (and thus the ratio is equivalent to the amplitude of the first trough on the autocorrelation function) and is centered at $t = 0$ (and thus the time separation is the same as the time of the first trough). Due to varying angle of incidence of different RFs,

in reality these two parameters are calculated for each of the RFs. Obviously, this procedure is applicable for reverberations with a single dominant frequency. After the removal of the reverberations, *PbS* and the Moho *Ps* phases show up clearly in the filtered RFs (Figure 2e). The direct *P* phase, which arrives at $t = 0$, is weaker than *PbS* and can barely be observed directly unless the frequency of the wavelet is unrealistically high.

2.3. Determination of Subsediment Crustal Thickness and V_P/V_S

The *H-k* stacking method [*Zhu and Kanamori*, 2000] can then be employed to estimate crustal thickness and V_P/V_S using the filtered RFs. However, due to the delay effects of the sedimentary layer, the conventional *H-k* stacking technique would result in a larger than real crustal thickness if time delays associated with the sedimentary layer are not corrected [*Yeck et al.*, 2013]. Here we use the arrival time of the *PbS* phase and the two-way traveltime of the reverberations to time correct the filtered RFs. The subsediment crustal thickness and V_P/V_S can be obtained by applying a time-corrected *H-k* stacking formula of the form

$$A(H_i, k_j) = \sum_{m=1}^{N} w_1 \times S_m \left(t_1^{(i,j)} + \delta t_m \right) + w_2 \times S_m \left(t_2^{(i,j)} + \Delta t_m - \delta t_m \right) - w_3 \times S_m \left(t_3^{(i,j)} + \Delta t_m \right), \tag{5}$$

where *i* and *j* are indexes for the candidate subsediment crustal thickness (H_i) and V_P/V_S (k_j), respectively, $A(H_i, k_j)$ is the stacking amplitude corresponding to the candidate pair of H_i and k_j, *N* is the number of RFs participated in the stacking, $S_m(t)$ is the amplitude of the point on the *m*th RF at time *t* after the direct *P* wave, w_1, w_2, and w_3 are weighting factors that satisfy $w_1 + w_2 + w_3 = 1$ [*Zhu and Kanamori*, 2000] for *PmS*, *PPmS*, and *PSmS* (Figure 1), respectively, δt_m is the time delay (relative to the direct *P* wave) of the *PbS* phase on the *m*th RF, Δt_m is the two-way traveltime of the reverberations obtained from autocorrelation of the *m*th RF, and $t_1^{(i,j)}$, $t_2^{(i,j)}$, and $t_3^{(i,j)}$ correspond to the theoretical moveout of *PmS*, *PPmS*, and *PSmS* phases in the subsediment crust. The optimal pair of H_i and k_j corresponds to the maximum amplitude of $A(H_i, k_j)$.

To better understand the time terms in equation (5), let us consider a hypothetical situation of vertical incidence, for which the delay time of the *PbS* phase, $\delta t = H_d/V_S - H_d/V_P$, and the reverberation period or two-way traveltime of *PbS*, $\Delta t = 2H_d/V_s$, where H_d is the thickness of the sedimentary layer. The *PmS* phase travels through the sedimentary layer once as an *S* wave (Figure 1c), and thus, the *S* and *P* wave differential time after traveling through the sedimentary layer is $H_d/V_S - H_d/V_P$, which is δt. The *PPmS* phase, on the other hand, has two *P* legs and an *S* leg in the sedimentary layer, and thus, the *S* and *P* wave differential traveltime is $H_d/V_S + 2H_d/V_P - H_d/V_P$ which happens to be $\Delta t - \delta t$. Finally, the *PSmS* phase has two *S* legs and one *P* leg in the sedimentary layer, and thus, the differential time is Δt. After the removal of the traveltimes associated with the low-velocity sedimentary layer, the station is virtually downward projected to the bottom of the sedimentary layer. Consequently, the optimal thickness and V_P/V_S of the subsediment crust are determined.

2.4. Determination of Sedimentary Thickness and V_P/V_S

We next propose a procedure to grid search for the optimal thickness and V_P/V_S of the sedimentary layer using the resulting subsediment crustal thickness and V_P/V_S. The phases that we use for this task are *PbS*, *PPmS*, and *PSmS* (note that the last two are not *PPbS* and *PSbS* which are too weak to be used, as discussed above). At first glance, it seems that *PPmS* and *PSmS* are associated with the Moho and not the sedimentary layer. However, because they travel through both the subsediment crustal and the sedimentary layers, their arrival times are functions of the thickness and V_P/V_S of both layers, as quantified in equations (7)–(9).

The grid search is conducted using

$$A(H_i, k_j) = \sum_{m=1}^{n} w_4 \times S_m(t_4^{(i,j)}) + w_2 \times S_m(t_2^{(i,j)}) - w_3 \times S_m(t_3^{(i,j)}), \tag{6}$$

where H_i and k_j indicate a pair of candidate sedimentary thickness and V_P/V_s, w_4, w_2, and w_3 are the weighting factors for *PbS*, *PPmS*, and *PSmS*, respectively, and $t_4^{(i,j)}$, $t_2^{(i,j)}$, and $t_3^{(i,j)}$ are the moveout of *PbS*, *PPmS*, and *PSmS* phases through the sedimentary and subsediment crustal layers calculated using the following equations:

$$t_4^{(i,j)} = \int_{-H_i}^{0} \left[\sqrt{\left(V_P(z)/k_j \right)^{-2} - p^2} - \sqrt{V_P(z)^{-2} - p^2} \right] dz, \tag{7}$$

$$t_2^{(i,j)} = \int_{-H_i}^{0} \left[\sqrt{\left(V_P(z)/k_j \right)^{-2} - p^2} + \sqrt{V_P(z)^{-2} - p^2} \right] dz + \int_{-(H_i+Hc)}^{-H_i} \left[\sqrt{\left(V_P(z)/k_c \right)^{-2} - p^2} + \sqrt{V_P(z)^{-2} - p^2} \right] dz, \tag{8}$$
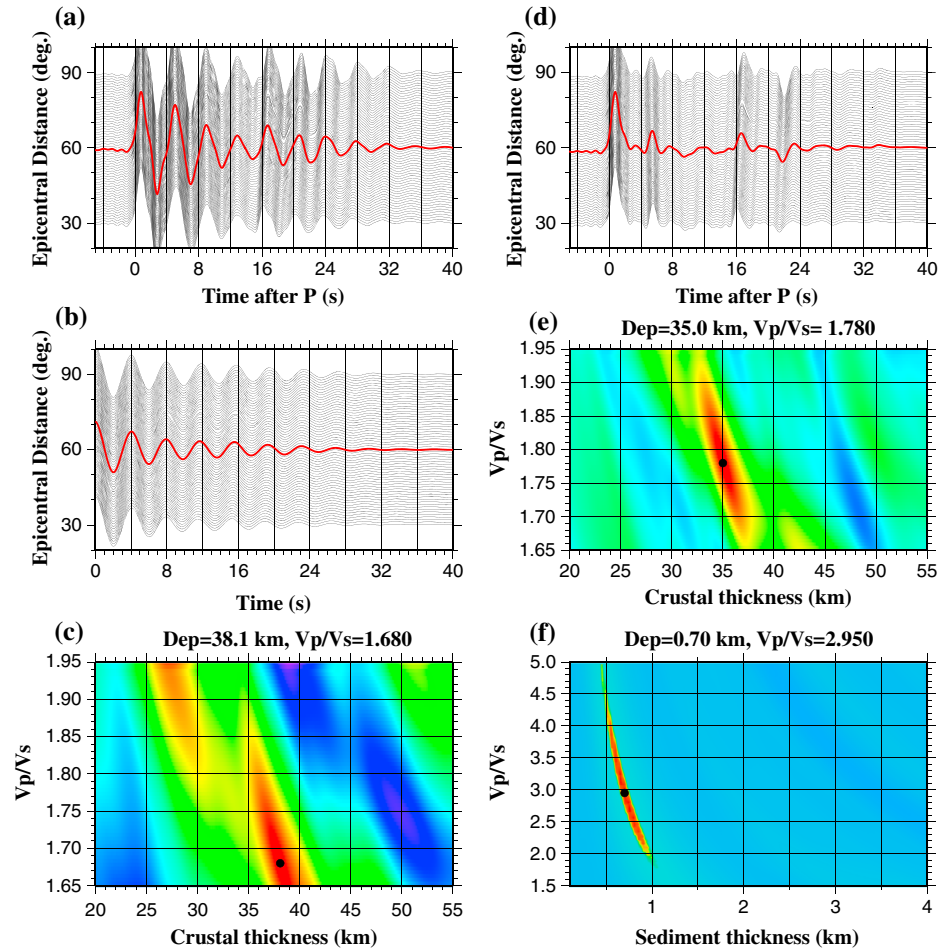
Figure 3. (a) Synthetic RFs plotted against epicentral distance. The red trace is the result of simple time domain summation (without moveout correction) of the individual traces. (b) Autocorrelations of each RFs in Figure 3a against epicentral distance. (c) Contour of stacking energy from *H-k* stacking using the RFs shown in Figure 3a. (d) Resulting RFs after the application of resonance removal filters. (e) Contour of stacking energy from $(H - k)_c$ stacking using the filtered RFs shown in Figure 3d. (f) Same as Figure 3e but for $(H - k)_d$ stacking.

and

$$t_3^{(i,j)} = \int_{-H_i}^{0} 2\sqrt{\left(V_P(z)/k_j\right)^{-2} - p^2}\,dz + \int_{-(H_i+Hc)}^{-H_i} 2\sqrt{\left(V_P(z)/k_c\right)^{-2} - p^2}\,dz, \tag{9}$$

where *i* and *j* are indexes corresponding to the candidate sedimentary thickness (H_i) and V_P/V_S (k_j), $V_P(z)$ is the *P* wave velocity at depth *z*, *p* is the ray parameter, and H_c and k_c are the subsediment crustal thickness and V_P/V_S, respectively, obtained from applying equation (5).

In order to distinguish the above two kinds of *H-k* stacking procedures (equations (5) and (6)), in the following we refer the grid search procedure (equation (5)) to image the subsediment crustal structure as $(H - k)_c$ stacking and that for the sedimentary structure (equation (6)) as $(H - k)_d$ stacking.

3. Synthetic Experiments

To test the above technique, we generate synthetic RFs using a reflectivity-based method [*Randall*, 1994] with a Gaussian wavelet of the form $\exp(-4t^2)$. The station is in a sedimentary basin, and the *i*th hypothetical event has an epicentral distance of $30 + i°$ where $i = 0, 1, ...60$. Synthetic RFs are generated using the following parameters: for the sedimentary layer, the thickness, V_P, V_S, V_P/V_S, and density are 0.7 km, 2.1 km/s, 0.7 km/s, 3.0, and 1970 kg/m³, respectively; for the subsediment crustal layer, the corresponding values are 35 km, 6.1 km/s, 3.49 km/s, 1.75, and 2700 kg/m³; and for the mantle, they are ∞, 8.0 km/s, 4.5 km/s, 1.78,
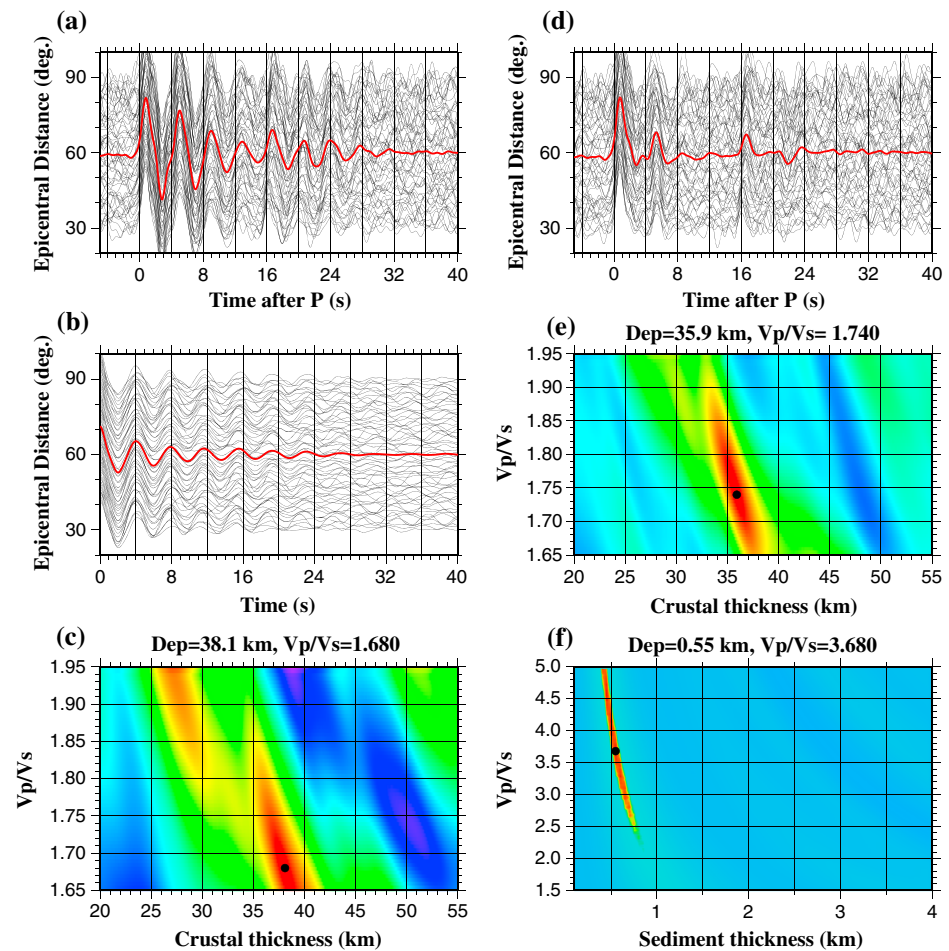
Figure 4. Same as Figure 3 but for a model with 15% random noise added in the RFs.

and 3300 kg/m³. On the synthetic RFs, the Moho *Ps* phases are completely masked by the strong near-surface reverberations (Figure 3a). *H-k* stacking without considering the sedimentary effects results in incorrect crustal thickness and V_P/V_S (Figure 3c). After applying the resonance removal filter, *PbS* and the Moho *Ps* phases are well recovered (Figure 3d).

The weighting factors in equations (5) and (6) are selected to maximize the resolution of the resulting optimal thickness and V_P/V_S values and are dependent on the relative amplitude of the phases involved and the rate of moveout with respect to the epicentral distance. For investigating the subsediment crustal structure, they are set as $w_1 = 0.5$, $w_2 = 0.4$, and $w_3 = 0.1$, and those for imaging the sedimentary structure, the selected values are $w_4 = 0.05$, $w_2 = 0.7$, and $w_3 = 0.25$. Ten bootstrap iterations are used to evaluate the standard deviations of the observed sedimentary and subsediment crustal parameters [*Efron and Tibshirani*, 1986; *Press et al.*, 1992; *Liu and Gao*, 2010].

The $(H-k)_c$ stacking technique is then applied on the filtered RFs to search for the optimal subsediment crustal thickness (in the range of 20–55 km with an interval of 0.1 km) and V_P/V_S (in the range of 1.65–1.95 with an interval of 0.01). The resulting subsediment crustal thickness is 35.0 km and the V_P/V_S is 1.78 (Figure 3e), which are nearly identical to the input parameters (35.0 km and 1.75) used to generate the RFs. Similarly, the optimal sedimentary layer thickness and V_P/V_S are searched using the $(H − k)_d$ stacking procedure in the depth range of 0–4 km with an interval of 0.05 km and in the V_P/V_S range of 1.50–5.00 with an interval of 0.01. The results are 0.70 km and 2.95, respectively (Figure 3f), which are almost the same as the input parameters of 0.7 km and 3.0. We next use noisy synthetic RFs to further test the techniques. Figure 4 shows results for a model in which the RFs are contaminated by random noise with a peak amplitude of 15% relative to the amplitude of the first peak. *H-k* stacking using the original RFs fails to obtain the correct results (Figure 4c). After applying the resonance removal filter, the resulting *H* and V_P/V_S for the subsediment crust (35.8 km and 1.74) and the
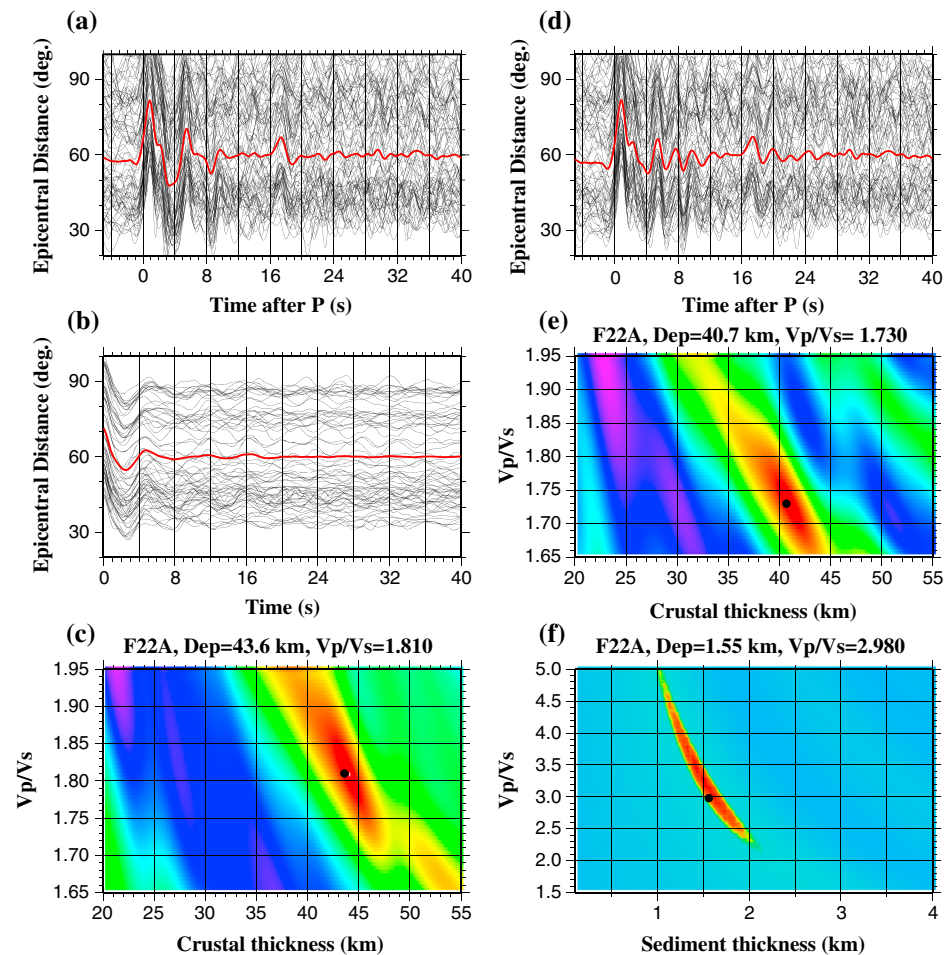
Figure 5. Same as the previous figure but for real data recorded by USArray station F22A located in the Powder River Basin, Wyoming.

sedimentary layer (0.55 km and 3.68) are similar to the parameters used to generate the noisy RFs (Figures 4e and 4f).

4. Testing Using Real Data

Our reverberation removal technique is further tested using RFs recorded by two broadband seismic stations. Station F22A is located in the Powder River Basin, northern Wyoming (USA), and has been studied by *Yeck et al.* [2013] using the sequential *H-k* stacking method, and station NE68 is situated in the Songliao Basin, northeast China, and has been investigated by *Tao et al.* [2014] based on the theory of wavefield continuation and decomposition. The stations were selected because they were used for testing different sediment-removal techniques and also have independent estimates of crustal thickness from active source seismic experiments.

Three-component data from the stations were requested from the Incorporated Research Institutions for Seismology (IRIS) Data Management Center. Earthquakes with epicentral distances in the range of 30–90° and with a magnitude of M_c or greater were used in the study, where M_c is defined as $5.2 + (\Delta - 30.0)/(180.0 - 30.0) - D/700.0$, in which Δ is the epicentral distance in degree and D is the focal depth in kilometer [*Liu and Gao*, 2010]. The seismograms were windowed at 20 s before and 260 s after the predicted direct *P* wave arrival calculated using the IASP91 Earth model. A band-pass filter in the frequency range of 0.04–0.8 Hz was applied to enhance the signals. An event was not used if the radial component has a signal-to-noise ratio (SNR) below 4.0. The selected seismograms were converted to radial RFs using the procedure of *Ammon* [1991], and an SNR-based procedure was applied to reject low-quality RFs. Detailed information about the seismogram and RF selection procedures including the definition of the SNRs can be found in *Gao and Liu* [2014].
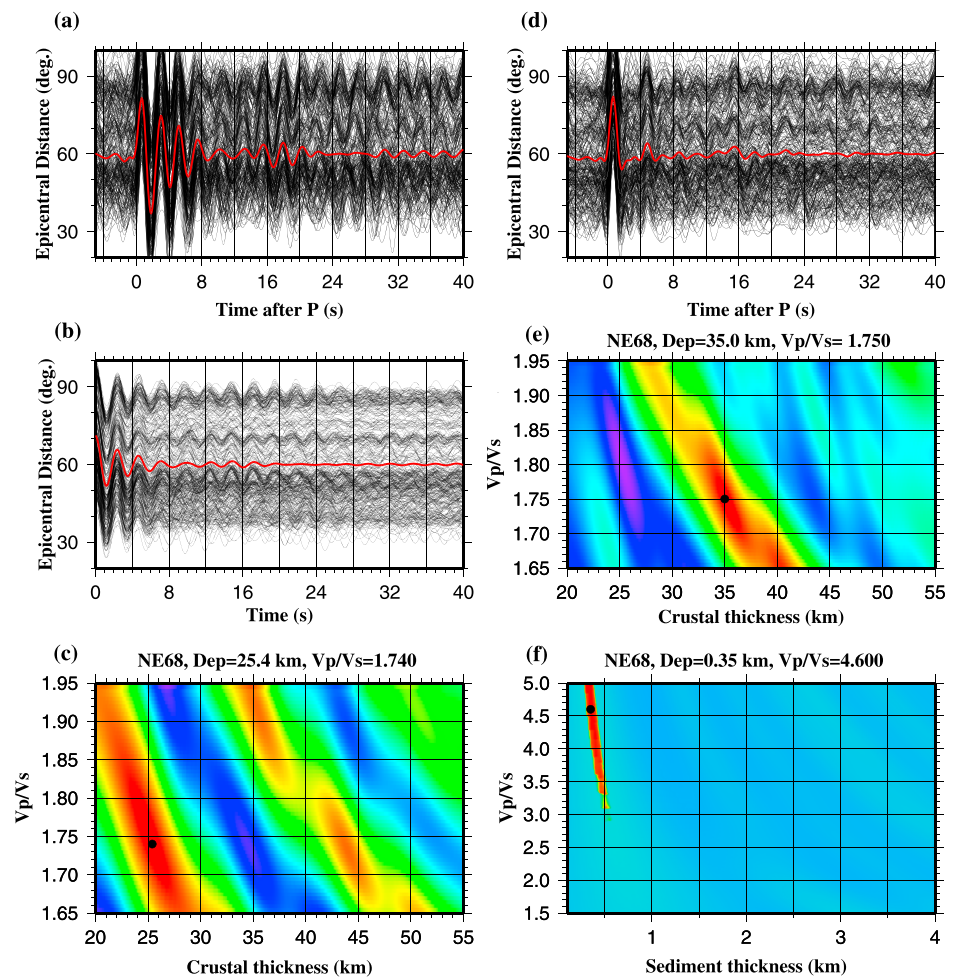
Figure 6. Same as the previous figure but for station NE68 in the Songliao Basin, northeast China.

4.1. Station F22A

For station F22A, we use the same *P* wave velocities for the sedimentary and subsediment crustal layers as those used in *Yeck et al.* [2013], which are 3.6 km/s and 6.7 km/s, respectively. The sedimentary V_P was taken from well logs [*Moore*, 1985], and the subsediment crustal V_P was obtained from nearby active source seismic studies [*Snelson et al.*, 1998]. On the original RFs (Figure 5a), there is a strong arrival at about 5 s with an amplitude of about 50% of that of the first peak. In addition, there is a strong trough between this arrival and the first peak. Both arrivals and the well-defined trough on the autocorrelation functions (Figure 5b) indicate the existence of a low-velocity sedimentary layer.

After applying the resonance removal filter to the original 89 RFs (Figure 5a), the Moho *Ps* phases are well revealed (Figure 5d). The strong amplitude at ∼5 s on the original RFs (Figure 5a) is caused by the accidental simultaneous arrival of the *PmS* and the first positive pulse of the reverberation of the *PbS* phase.

Application of the $(H - k)_c$ stacking procedure leads to a subsedimentary crustal thickness of 40.7 ± 0.2 km and a V_P/V_S of 1.73 ± 0.01 (Figure 5e), which are comparable with the values of 40.5 ± 0.6 km and 1.77 ± 0.01 obtained by *Yeck et al.* [2013]. The obtained subsediment crustal thickness is also consistent with that from active source seismic studies [*Snelson et al.*, 1998], which reported a value of about 40 km. The resulting sedimentary thickness and V_P/V_S are 1.5 ± 0.07 km and 3.13 ± 0.14, respectively (Figure 5f), which are similar to the results of 2.1 ± 0.08 km and 2.54 ± 0.07 reported by *Yeck et al.* [2013]. The slight mismatch between our results and those obtained by *Yeck et al.* [2013] could be resulted from different approaches and parameters used for data selection, processing, and RF stacking.

4.2. Station NE68

Station NE68 has 362 high-quality RFs with significantly better developed reverberations than F22A. On the original RFs, the Moho Ps phases are completely masked by the strong near-surface reverberations (Figure 6a). Following *Tao et al.* [2014], we use an average P wave velocity of 2.1 km/s for the sedimentary layer and 6.4 km/s for the subsediment crust. After applying the resonance removal filter, the near-surface reverberations are effectively suppressed, and consequently, the Moho Ps phases are clearly observed (Figures 6d). Results from $(H-k)_c$ stacking using the filtered RFs are almost identical to those obtained by *Tao et al.* [2014], who reported a subsediment crustal thickness of 35.0 km and V_P/V_S of 1.730, and our $(H-k)_c$ stacking yields 35.2 ± 0.2 km and 1.74 ± 0.01 (Figure 6e), respectively. Similarly, the resulting sedimentary thickness and V_P/V_S using $(H-k)_d$ stacking are 0.35 ± 0.00 km and 4.61 ± 0.02 (Figure 6f), which are consistent with those obtained by *Tao et al.* [2014] (0.31 km and 4.118). The observed thickness of the low-velocity sedimentary layer also agrees well with the results from an active source seismic experiment [*Feng et al.*, 2010].

5. Discussion and Conclusions

The resulting high V_P/V_S values for stations NE68 and F22A can be caused by a poorly consolidated sedimentary layer. High V_P/V_S of such a layer has been observed elsewhere. For instance, beneath the Horn River Basin in northeast British Columbia, Canada, well-logging and active source seismic data revealed high V_P/V_S values ranging from about 2.5 to 5.5 in the top 500 m of the basin [see *Zuleta-Tobon*, 2012, Figures 4 and 5]. Laboratory experiments [*Prasad et al.*, 2004] indicate that V_P/V_S values are related to water content, amount of clay minerals, and the overlying pressure. The high sedimentary V_P/V_S values observed at stations NE68 and F22A suggest water saturation, high clay content, and perhaps low overlying pressure in the Songliao and Powder River basins.

The strong reverberations in the radial RFs caused by a low-velocity sedimentary layer can be effectively removed by applying the resonance removal filter to decipher the Ps phases associated with the Moho and the P-to-S converted phase from the bottom of the sedimentary layer. Tests using synthetic and real data indicate that the proposed technique can efficiently obtain the thickness and V_P/V_S of both the sedimentary layer and the subsediment crust with high reliability. Contrary to most other techniques, which favor the absence or weak sedimentary reverberations, the proposed technique leads to more accurately determined results with stronger reverberations, thanks to the better defined parameters needed by the resonance removal filter associated with stronger reverberations. Also, the technique is computationally inexpensive and thus can be applied to large data sets such as those recorded by the USArray.

Obviously, the existence of strong reverberations of at least a couple of cycles is needed in order for the proposed technique to be applied successfully. Testing using data from numerous stations suggests that as long as the RFs have reverberations with a dominant frequency, the technique can successfully remove the reverberations. Such reverberations cannot be generated if the sedimentary layer is thinner than about one fourth of the wavelength of the PbS phase. If we assume a sedimentary S wave velocity of 0.33 km/s and a period of 3 s, the required minimum thickness is about 0.25 km. On the other hand, if the sedimentary layer is too thick (e.g., thicker than 5–8 km, depending on the attenuation factor), the reverberations decay rapidly with time, leading to poorly defined resonance removal filters. A thick sedimentary layer is characterized by RFs with abnormally low frequencies and a large delay of the PbS phase. Another potential problem for a very thick sedimentary layer is that the impedance contrast across the basin bottom may be too small (due to gravitational compaction) to generate significant reverberations. Furthermore, the technique is not expected to perform well if there are strong interfaces inside the sedimentary layer. Such interfaces produce complicated interactions between the reverberations in two or more layers, and modifications to equation (2) and other steps of the technique are needed to account for such a scenario. Finally, cautions must be taken for stations near the edge of sedimentary basins or in areas with significant undulations of the basin bottom. Due to the rapid lateral variation in the thickness of the sedimentary layer, the two-way traveltime of the reverberations could be dependent on the arriving direction of the seismic waves. In such a case, the above technique can be applied to events from narrow azimuthal bands.

References

Ammon, C. J. (1991), The isolation of receiver effects from teleseismic P waveforms, *Bull. Seismol. Soc. Am.*, *81*, 2504–2510.

Anandakrishnan, S., and J. P. Winberry (2004), Antarctic subglacial sedimentary layer thickness from receiver function analysis, *Global Planet. Change*, *42*, 167–176, doi:10.1016/j.gloplacha.2003.10.005.

Bashir, L., S. S. Gao, K. H. Liu, and K. Mickus (2011), Crustal structure and evolution beneath the Colorado Plateau and the southern Basin and Range Province: Results from receiver function and gravity studies, *Geochem. Geophys. Geosyst.*, *12*, Q06008, doi:10.1029/2011GC003563.

Bostock, M. G., and A. M. Trehu (2012), Wave-field decomposition of ocean bottom seismograms, *Bull. Seismol. Soc. Am.*, *102*, 1681–1692, doi:10.1785/0120110162.

Burdick, L. J., and C. A. Langston (1977), Modeling crustal structure through the use of converted phases in teleseismic body-wave forms, *Bull. Seismol. Soc. Am.*, *67*, 677–691.

Chevrot, S., and R. D. Van der Hilst (2000), The Poisson's ratio of the Australian crust: Geological and geophysical implications, *Earth Planet. Sci. Lett.*, *183*, 121–132, doi:10.1016/S0012-821X(00)00264-8.

Clitheroe, G., O. Gudmundsson, and B. L. N. Kennett (2000), Sedimentary and upper crustal structure of Australia from receiver functions, *Aust. J. Earth Sci.*, *47*, 209–216.

Efron, B., and R. Tibshirani (1986), Bootstrap methods for standard errors, confidence intervals, and other measures of statistical accuracy, *Stat. Sci.*, *1*, 54–75.

Feng, Z., C. Jia, X. Xie, S. Zhang, Z. Feng, and T. A. Cross (2010), Tectonostratigraphic units and stratigraphic sequences of the nonmarine Songliao Basin, northeast China, *Basin Res.*, *22*, 79–95, doi:10.1111/j.1365-2117.2009.00445.x.

Gao, S. S., and K. H. Liu (2014), Mantle transition zone discontinuities beneath the contiguous United States, *J. Geophys. Res. Solid Earth*, *119*, 6452–6468, doi:10.1002/2014JB011253.

He, C., S. Dong, and X. Chen (2012), Seismic technique for studying sedimentary layer: Bohai Basin as an example, *Acta Geol. Sin.*, *86*, 1105–1115, doi:10.1111/j.1755-6724.2012.00734.x.

Langston, C. A. (1979), Structure under Mount Rainier, Washington, inferred from teleseismic body waves, *J. Geophys. Res.*, *84*, 4749–4762, doi:10.1029/JB084iB09p04749.

Langston, C. A. (2011), Wave-field continuation and decomposition for passive seismic imaging under deep unconsolidated sediments, *Bull. Seismol. Soc. Am.*, *101*, 2176–2190, doi:10.1785/0120100299.

Leahy, G. M., R. L. Saltzer, and J. Schmedes (2012), Imaging the shallow crust with teleseismic receiver functions, *Geophys. J. Int.*, *191*, 627–636, doi:10.1111/j.1365-246X.2012.05615.x.

Liu, K. H., and S. S. Gao (2010), Spatial variations of crustal characteristics beneath the Hoggar swell, Algeria, revealed by systematic analyses of receiver functions from a single seismic station, *Geochem. Geophys. Geosyst.*, *11*, Q08011, doi:10.1029/2010GC003091.

Mandal, P. (2006), Sedimentary and crustal structure beneath Kachchh and Saurashtra regions, Gujarat, India, *Phys. Earth Planet. Inter.*, *155*, 286–299, doi:10.1016/j.pepi.2006.01.002.

Moore, W. R. (1985), Seismic profiles of the Powder River basin, Wyoming, in *Seismic Exploration of the Rocky Mountain Region*, edited by R. R. Griesand and R. C. Dyer, pp. 187–200, Rocky Mt. Assoc. of Geol., Denver, Colo.

Nair, S. K., S. S. Gao, K. H. Liu, and P. G. Silver (2006), Southern African crustal evolution and composition: Constraints from receiver function studies, *J. Geophys. Res.*, *111*, B02304, doi:10.1029/2005JB003802.

Owens, T. J., G. Zandt, and S. R. Taylor (1984), Seismic evidence for an ancient rift beneath the Cumberland Plateau, Tennessee: A detailed analysis of broadband teleseismic *P* waveforms, *J. Geophys. Res.*, *89*, 7783–7795, doi:10.1029/JB089iB09p07783.

Prasad, M., M. A. Zimmer, P. A. Berge, and B. P. Bonner (2004), Laboratory measurements of velocity and attenuation in sediments, *LLNL Rep. UCRL-JRNL-205155*, 34 pp., Lawrence Livermore Natl., Lab.Livermore, Calif.

Press, W. H., S. A. Teukolsky, W. T. Vetterling, and B. P. Flannery (1992), Numerical recipes in FORTRAN, Cambridge Univ. Press.

Randall, G. (1994), Efficient calculation of complete differential seismograms for laterally homogeneous Earth models, *Geophys. J. Int.*, *118*, 245–254, doi:10.1111/j.1365-246X.1994.tb04687.x.

Reed, C. A., S. Almadani, S. S. Gao, A. Elsheikh, S. Cherie, M. Abdelsalam, A. Thurmond, and K. H. Liu (2014), Receiver function constraints on crustal seismic velocities and partial melting beneath the Red Sea rift and adjacent regions, Afar Depression, *J. Geophys. Res. Solid Earth*, *119*, 2138–2152, doi:10.1002/2013JB010719.

Sheehan, A. F., G. A. Abers, C. H. Jones, and A. L. Lerner-Lam (1995), Crustal thickness variations across the Colorado Rocky Mountains from teleseismic receiver functions, *J. Geophys. Res.*, *100*, 20,391–20,404, doi:10.1029/95JB01966.

Snelson, C. M., T. J. Henstock, G. R. Keller, K. C. Miller, and A. Levander (1998), Crustal and uppermost mantle structure along the Deep Probe seismic profile, *Rocky Mt Geol.*, *33*, 181–198, doi:10.2113/33.2.181.

Stoffa, P. L., P. Buhl, and G. Bryan (1974), The application of homomorphic deconvolution to shallow-water marine seismology—Part I: Models, *Geophysics*, *39*, 401–416, doi:10.1190/1.1440438.

Tao, K., T. Z. Liu, J. Y. Ning, and F. Niu (2014), Estimating sedimentary and crustal structure using wavefield continuation: Theory, techniques and applications, *Geophys. J. Int.*, *197*, 443–457, doi:10.1093/gji/ggt515.

Thorwart, M., and T. Dahm (2005), Wavefield decomposition for passive ocean bottom seismological data, *Geophys. J. Int.*, *163*, 611–621, doi:10.1111/j.1365-246X.2005.02761.x.

Yeck, W. L., A. F. Sheehan, and V. Schulte-Pelkum (2013), Sequential H-k stacking to obtain accurate crustal thicknesses beneath sedimentary basins, *Bull. Seismol. Soc. Am.*, *103*, 2142–2150, doi:10.1785/0120120290.

Yilmaz, O. (2001), *Seismic Data Analysis: Processing, Inversion and Interpretation of Seismic Data*, Soc. Explor. Geophysicists, Tulsa, Okla.

Zandt, G., and C. J. Ammon (1995), Continental crust composition constrained by measurements of crustal Poisson's ratio, *Nature*, *374*, 152–154, doi:10.1038/374152a0.

Zelt, B. C., and R. M. Ellis (1999), Receiver-function studies in the Trans-Hudson orogen, Saskatchewan, *Can. J. Earth Sci.*, *36*, 585–603.

Zhu, L., and H. Kanamori (2000), Moho depth variation in Southern California from teleseismic receiver functions, *J. Geophys. Res.*, *105*, 2969–2980, doi:10.1029/1999JB900322.

Zuleta-Tobon, L. M. (2012), Near-surface characterization and Vp/Vs analysis of a shale gas basin, MS thesis, Univ. Calgary, Canada. [Available at http://hdl.handle.net/1880/48952.]